Catalysis Today 171 (2011) 266–274

Contents lists available at ScienceDirect

Catalysis Today

journal homepage: www.elsevier.com/locate/cattod

Synthesis gas conversion over a Rh–K–MoP/SiO_2 catalyst

Sharif F. Zaman, Kevin J. Smith*

Department of Chemical & Biological Engineering, University of British Columbia, 2360 East Mall, Vancouver, BC, Canada V6T 1Z3

ARTICLE INFO

Article history:
Received 8 September 2010
Received in revised form 4 February 2011
Accepted 16 February 2011
Available online 21 March 2011

Keywords:
Catalyst
Promoter
Synthesis gas
Gas-to-liquid
Ethanol
Acetaldehyde
Kinetics
MoP
Rhodium
Potassium

ABSTRACT

Synthesis gas conversion over a 1 wt% Rh–5 wt% K–10 wt% MoP on SiO_2 catalyst was investigated at different temperatures, synthesis gas H_2/CO ratios and space velocities. Compared to a 5 wt% K–10 wt% MoP on SiO_2 catalyst, addition of Rh increased the stability of the catalyst and the selectivity to hydrocarbons. The highest C_{2+} oxygenate selectivity of 44 C atom% was achieved at 598 K and H_2:CO = 1. Power law kinetics were used to describe the space–time yield (STY) of the major products. The apparent activation energies for ethanol (77.7 kJ/mol) and acetaldehyde (81.9 kJ/mol) formation suggested that both originated from the same surface intermediate whereas, a higher activation barrier was identified for methanol (114.5 kJ/mol).

1. Introduction

Interest in the development of new technologies that convert renewable resources to alternative transportation fuels, and thereby address issues of air quality, CO_2 emissions and energy security, are increasing. Biomass, especially agricultural and forest residue, has potential as a renewable energy resource and is expected to play an important role in the synthesis of clean and sustainable fuels [1,2]. One route to clean fuels from biomass is through the thermocatalytic conversion of synthesis gas ($CO + CO_2 + H_2$) that is produced by biomass gasification. The synthesis of alcohols from synthesis gas (syngas) has been known since the 1930s [3,4] and the production of methanol is practiced industrially using Cu/ZnO catalysts [5]. Higher alcohols, especially iso-butanol, are produced when high temperature Zn/Cr and low temperature Cu/ZnO methanol catalysts are promoted with alkali metals. These catalysts produce C_1–C_6 linear and branched alcohols [6,7] primarily via an aldol condensation or methanol homologation reaction mechanism [1,8]. However, they have very low selectivity toward ethanol because of the fast C–C chain growth of the C_2 surface intermediate [8,9].

Many other catalysts for the synthesis of ethanol or mixed alcohols have been reported in the literature, and these can be categorized as (i) modified Fischer–Tropsch (FT) catalysts (ii) Rh-based catalysts and (iii) Mo-based catalysts. Alkali-doped FT catalysts produce mainly hydrocarbons from syngas, with a ratio of hydrocarbon to alcohol equal to one or more [10], and among the alcohols, C_{2+} alcohols predominate. A high yield of alcohols has also been reported on Cu–Co catalysts, but these catalysts produce significant amounts of hydrocarbons which have a negative effect on the overall process feasibility, especially if the CH_4 selectivity is above about 10% [1]. Rh-based catalysts have the highest reported ethanol selectivity among the various synthesis gas catalysts investigated to date [1,11–16]. Hu et al. reported 44.5 C atom% selectivity to ethanol with a considerable amount of CH_4 (48 C atom%) in the product [11] when synthesis gas was reacted over a Rh catalyst, promoted with Li and Mn, at 573 K, 3 MPa and a syngas H_2:CO ratio of 2. Recently, Rh supported on carbon nanotubes was reported to have good selectivity (52.4 C atom%) towards C_{2+} oxygenates as well [12].

The high hydrocarbon selectivity reported on Rh-based catalysts, especially toward CH_4, means that these catalysts would be difficult to implement in a commercial process. Furthermore, because of cost and supply issues associated with Rh, there is significant interest in less expensive synthesis gas conversion catalysts with high alcohol selectivity. Several researchers have reported that Mo sulphides, phosphides, nitrides and carbides have catalytic

* Corresponding author. Tel.: +1 604 822 3601; fax: +1 604 822 6003.
E-mail address: kjs@interchange.ubc.ca (K.J. Smith).

0920-5861/$ – see front matter © 2011 Elsevier B.V. All rights reserved.
doi:10.1016/j.cattod.2011.02.017

properties similar to some precious metal [17], and that they resist sulphur poisoning [1]. These two characteristics have led to several studies of Mo-based catalysts for syngas conversion to alcohols. Synthesis gas conversion at 568 K, 7.2 MPa and a H_2:CO ratio of 1 was reported with high selectivity to ethanol (40 C atom%) over a K-promoted MoS_2 [18,19], but later researchers only achieved 10–30 C atom% ethanol selectivity on K–MoS_2 catalysts promoted with Rh, Co, Ni, and Mn [20–23]. Recently, syngas conversion over β-Mo_2C at 573 K and 8 MPa was reported to produce hydrocarbons and alcohols, and among the liquid products, ethanol predominated [24,25]. On alkali doped Mo catalysts (both Mo_2C and MoS_2), the higher alcohol synthesis followed the Anderson–Schulz–Flory distribution, with a high selectivity to methanol. Addition of FT metals (Ni, Co, Rh) increased the selectivity to ethanol and enhanced the performance of MoS_2 and Mo_2C catalysts [20–23,25].

The kinetics of synthesis gas conversion to alcohols has also been reported in the literature. The activation energy of synthesis gas conversion on Rh catalysts promoted with Mn has been reported by several researchers [13–16], with values of 90–140 kJ/mol reported for the activation energy of methane formation and 40–70 kJ/mol for ethanol formation. Kinetic models for higher alcohol synthesis over MoS_2 have also been developed by several researchers [26–28] and it is now well established that the alcohol chain growth occurs via a CO insertion mechanism on MoS_2 catalysts, although recent theoretical studies have shown that CO does not dissociate on MoS_2 [29]. There is very limited information on the kinetics of synthesis gas conversion over Mo_2C catalysts, although Xiang et al. [25] has reported the activation energies for linear alcohols (C_1–C_5) over several alkali-promoted Mo_2C catalysts. For K–Mo_2C the ethanol activation energy was 74 kJ/mol, and with the addition of Co, the activation energy decreased to 71 kJ/mol [25].

Recently, the present authors reported on the product distribution obtained from synthesis gas conversion over a new series of K–MoP catalysts supported on SiO_2 [30,31]. Within the investigated range of compositions, a 5 wt% K–10 wt% MoP supported on SiO_2 catalyst showed the highest selectivity towards liquid oxygenates and C_2 oxygenates, i.e. ethanol (16 C atom%) and acetaldehyde (18 C atom%). Although the MoP catalysts showed promising selectivity to oxygenates and ethanol, the catalysts deactivated during the first 20 h of operation before stabilizing at a lower level of conversion. In the present study, we demonstrate that addition of 1 wt% Rh to the 5 wt% K–10 wt% MoP-SiO_2 catalyst stabilizes the CO conversion. The space–time–yield data for the Rh–K–MoP/SiO_2 catalyst, measured at similar CO conversions (10–25%), have been used to develop simplified power law kinetic models of the synthesis of the oxygenated compounds and the apparent activation energies obtained for the Rh–K–MoP/SiO_2 catalyst have been compared to those obtained over other Mo catalysts.

2. Experimental

2.1. Catalyst preparation

The silica supported Rh–K–MoP catalyst was prepared by stepwise impregnation of a SiO_2 support, followed by calcination and temperature-programmed reduction (TPR). Approximately 10 g of the SiO_2 (Sigma–Aldrich, Grade 62, 60–200 mesh, BET area = 330 m^2/g, pore volume = 1.2 cm^3/g) was impregnated with a solution of potassium nitrate (1.77 g KNO_3, BDH Chemicals, 99.97% dissolved in 15 ml of de-ionized water). After aging at room temperature for 12 h, the impregnated SiO_2 was dried at 373 K for 12 h followed by calcination at 773 K for 5 h. Stoichiometric amounts (Mo:P = 1) of ammonium heptamolybdate (1.39 g of $(NH_4)_6Mo_7O_{24}$ $4H_2O$, BDH Chemicals, 99%) and diammonium hydrogen phosphate (1.04 g of $(NH_4)_2HPO_4$, Sigma–Aldrich, 99%) were dissolved in 15.7 ml of de-ionized water and impregnated drop-wise onto 10 g of the K–SiO_2 with continuous mixing. The impregnated support was held at room temperature for 12 h before being dried at 373 K for 12 h and calcined at 773 K for 5 h. To add the 1 wt% Rh, 0.215 g of rhodium (III) acetate (Sigma–Aldrich, 99%) was dissolved in 15 ml of de-ionized water. A few drops of HNO_3 were added to make a translucent solution (light brown-yellow in color). The Rh solution was then added to the calcined K–MoP–SiO_2, aged for 12 h at room temperature and dried at 373 K for 12 h. A final calcination was conducted at 773 K for 5 h. The calcined catalyst precursor was subjected to TPR in a H_2 (Praxair, 99.99%) flow of 120 cm^3 (STP) min^{-1} g^{-1}, at a temperature ramp of 1 K/min to a final temperature of 923 K. The final temperature was maintained for 2 h. After reduction, the catalyst was cooled in He to the desired reaction temperature. For samples prepared for EDX, XPS and BET area analysis, the catalyst was cooled to room temperature in He and then passivated in 2 vol% O_2 in He for 2 h at room temperature prior to removal from the reactor.

Details of the preparation of the MoP/SiO_2 and K–MoP/SiO_2 catalysts used herein for comparison, have been reported previously [30,31].

2.2. Catalyst characterization

The chemical composition of the prepared catalysts was done by CANTEST Laboratories (Burnaby, BC) using ICP-AES. Prior to analysis about 0.1 g of the passivated catalyst was mixed with 0.7 g of $LiBO_2$ and fused at 1273 K before being dissolved in 100 ml of 4% nitric acid.

The catalyst single point BET surface areas were measured using a Micromeritics FlowSorbII 2300 analyser. About 0.1 g of the passivated catalyst was degassed at 473 K for 2 h and the measurement was made using 30% N_2 and 70% He. Temperature-programmed reduction experiments were carried out using a Micromeritics AutoChem 2920 apparatus, following the procedure of Zuzaniuk and Prins [33]. The calcined, catalyst precursor (160–180 mg) was placed in a quartz U-tube and reduced in a flow of a 9.5% H_2/Ar mixture (50 ml min^{-1}). The temperature was increased at a ramp rate of 5 K min^{-1} up to 1023 K, the final temperature being maintained for 4 h. Prior to the analysis, the temperature-programmed reduction of a reference material (silver oxide) was carried out using the same procedure. The peak area of the reference material was correlated to the known volume of consumed H_2 and these data were used to calculate H_2 consumption during the reduction of the phosphide precursors.

EDX analysis was performed using a Hitachi S-3000N electron microscope operated with a 20 kV electron beam acceleration voltage. The average composition, from at least 10 data points, was determined for each catalyst sample. A Leybold Max200 X-ray photoelectron spectrometer with an Al Kα photon source was used for the XPS analysis. After reduction and reaction the catalyst was cooled to room temperature in He and prior to removal from the reactor, the catalyst was passivated in 2 vol% O_2 in He for 2 h at room temperature. Exposure of the samples to ambient atmosphere was minimized by transferring the samples from the reactor to the spectrometer either in vacuum or under N_2. No further treatment of the catalysts was done in the XPS chamber. All XPS spectra were corrected to the C1s peak with a binding energy (BE) of 284.6 eV.

2.3. Catalyst assessment

Catalyst activities were measured in a laboratory fixed-bed micro-reactor (copper lined stainless steel tube with o.d. = 9.53 mm and i.d. = 6.35 mm), operated at low conversion to investigate the

Table 1
Comparison of MoP catalyst compositions.

	Nominal (fresh catalyst), wt%	Measured – EDX (fresh catalyst), wt%	Measured – ICP-AES (after reaction), wt%
MoP/SiO_2			
MoP	10	7.80[a]	8.30[a]
SiO_2	90	92.70	91.70
Mo:P	1.00	0.70	1.02
$K–MoP/SiO_2$			
K_2O	5	5.80	5.5
MoP	10	8.50[a]	10.6[a]
SiO_2	85	85.60	83.9
Mo:P	1.00	0.72	1.10
$Rh–K–MoP/SiO_2$			
Rh	1	1.12	0.85
K_2O	5	4.45	5.00
MoP	10	9.15[a]	9.40[a]
SiO_2	84	85.28	84.80
Mo:P	1.00	0.76	1.04

[a] Based on the Mo analysis.

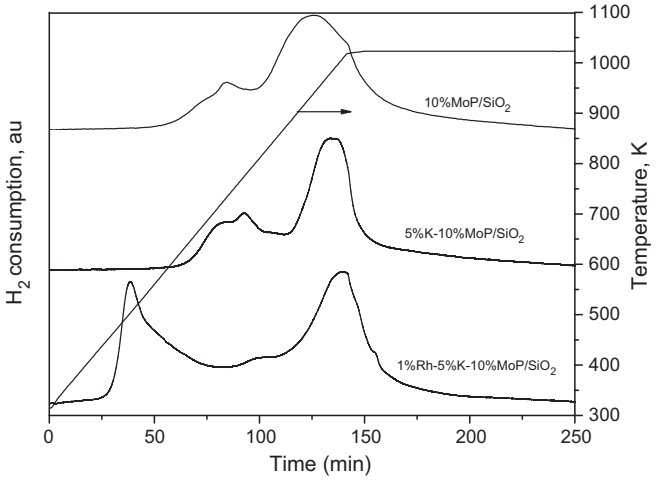

Fig. 1. TPR profile of MoP/SiO_2, $K–MoP/SiO_2$ and $Rh–K–MoP/SiO_2$ catalyst.

kinetics of the reaction. This was achieved by adjusting the gas hourly space velocity (GHSV) at each reaction temperature. Accordingly, at 573 K, 598 K and 613 K, the GHSV was set at 3960, 7920 and 15,840 h^{-1}, by using 1, 0.5 and 0.25 g catalyst, respectively. The calcined catalyst particles (average diameter = 150 μm) were placed on a packed bed of quartz wool inside the reactor and held in place by a bed of quartz beads. Prior to the start of the reaction the calcined catalyst was reduced *in situ* in 120 (STP) $cm^3\ min^{-1}\ g^{-1}$ of H_2 at a temperature ramp rate of 1 K/min to a final temperature of 923 K that was held for 2 h before cooling the reactor to the desired reaction temperature in He. The catalyst bed depth was 2–7 cm and calculation showed that this configuration ensured plug-flow through the reactor. A high temperature back pressure regulator was used to control the reactor pressure and a mass flow controller was used to control the flow of pre-mixed gas to the reactor. Various H_2:CO gas mixtures were investigated. The reaction products were analyzed using an in-line gas chromatograph (GC). Light gases (CO, CO_2 and $C_1–C_4$ hydrocarbons) were separated using a 5 m temperature-programmed Porapak Q 80/100 packed column and quantified with a thermal conductivity detector. The alcohols, aldehydes, ketones, carboxylic acids and C_5 + hydrocarbons were separated using a 30 m temperature-programmed EC™-wax capillary column (i.d. = 0.53 mm and film thickness 1.20 μm) and quantified using a flame ionization detector. GC/MS analysis was also carried out periodically to confirm the identity of the reaction products.

The activities of the catalysts were measured at different temperatures and GHSVs and at each condition the catalysts were evaluated for a period of at least 60 h of continuous operation. Some experiments were repeated to quantify the experimental error and analysis showed the conversion and selectivity data to be within ± 10% of the reported values. Calculation of the internal and external heat and mass transfer rates, and application of the Mears and Weisz–Prater criteria, confirmed that at the conditions of the experiments, the reactor operated free of significant heat and mass transfer resistances. The carbon balance across the reactor was >98% for all the experimental data reported herein.

3. Results

3.1. Catalyst characterization

Table 1 reports the compositions of the MoP/SiO_2, the $K–MoP/SiO_2$ and the $Rh–K–MoP/SiO_2$ catalysts used in the present study. Chemical analysis (ICP-AES) of the catalysts after reaction was in good agreement with the nominal catalyst compositions. After reaction, the catalysts were marginally enriched in Mo, possibly a consequence of some P loss during temperature programmed reduction of the calcined catalyst precursors, as reported by Clark and Oyama [32]. Table 1 also shows that the catalyst compositions, as determined by EDX, were in reasonable agreement with the ICP-AES chemical analysis, except that the P content was over estimated by EDX (Mo:P ratio < 1 in all cases) because of poor resolution of the Si and P peaks.

The TPR profile of the calcined $Rh–K–MoP/SiO_2$ catalyst precursor is compared to that obtained from the MoP/SiO_2 and $K–MoP/SiO_2$ catalyst precursors in Fig. 1. After calcination, it was assumed that the Mo and P of the catalyst precursors were completely oxidized and present on the support as Mo^{6+} and P^{5+}, respectively. The TPR profile of the 10 wt% $MoP–SiO_2$ catalyst was in agreement with that reported by Zuzaniuk and Prins [33] with two peak maxima at 727 and 938 K and a characteristic low temperature shoulder at about 700 K. The low temperature peaks were assigned to the reduction of Mo^{6+} species to Mo^{4+} [34], while the large peak at 938 K was assumed to result from the overlapping of several peaks, corresponding to the reduction of Mo^{4+} to Mo^0 and of P^{5+} to P^0. For the 5 wt% K–10 wt% MoP/SiO_2 catalyst, the peaks shifted to higher temperature compared to the 10 wt% MoP, with peak maxima at 773 and 976 K, and these peak maxima were also present in the 1 wt% Rh–5 wt% K–10 wt% MoP/SiO_2 catalyst. The $Rh–K–MoP/SiO_2$ catalyst also showed a new reduction peak at about 505 K that was not present in the TPR profiles of the $K–MoP/SiO_2$ and MoP/SiO_2 catalysts, and was assigned to the reduction of Rh_2O_3 [15,35,36]. From the TPR analysis, there was no clear indication of a strong interaction between the Rh and the MoP since there was no shift in the reduction peak temperatures of the Mo or Rh precursors. The reduction of Rh_2O_3 was assumed to follow the reaction stoichiometry $Rh_2O_3 + 3H_2 \rightarrow 2Rh + H_2O$ and the stoichiometric H_2 consumption required to reduce the Rh present on the 1 wt% Rh–5 wt% K–10 wt% $MoP–SiO_2$ catalyst precursor was 145.7 μmol H_2/g. The difference between the total H_2 consumed for the $K–MoP/SiO_2$ and the $Rh–K–MoP/SiO_2$ catalyst precursors corresponded to 100% reduction of the Rh_2O_3.

The reduction of Mo and P species from their high oxidation state, Mo^{6+} and P^{5+} present after calcination, was assumed to follow the reaction $2MoO_3{\cdot}P_2O_5 + 11H_2 \rightarrow 2MoP + 11H_2O$. Accordingly, the degrees of reduction calculated from Fig. 1 were 78%, 73% and 66% for the 10 wt% MoP/SiO_2 catalyst, the 5 wt% K–10 wt% MoP/SiO_2 catalyst and the 1 wt% Rh–5 wt% K–10 wt% MoP/SiO_2, respectively. However, as noted in several previous studies of supported metal phosphide catalysts [37–40], the stoichiometry of

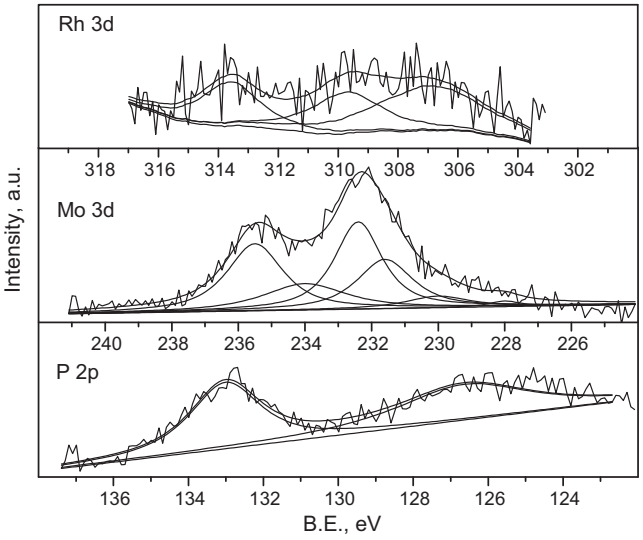

Fig. 2. XPS plots for reduced and passivated Rh–K–MoP/SiO_2 catalyst.

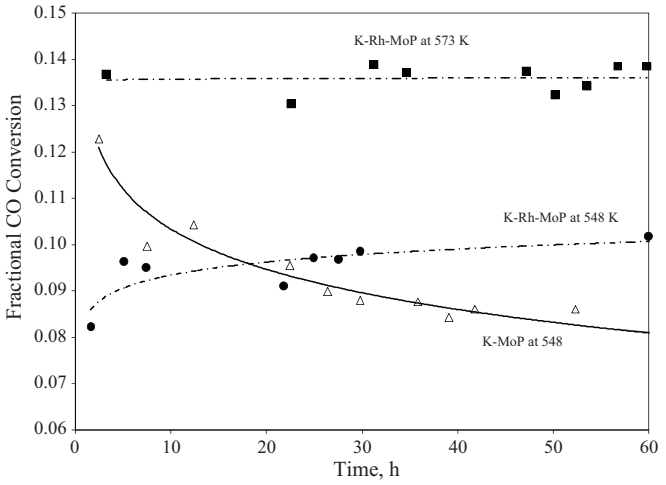

Fig. 3. Comparison between K–MoP and Rh–K–MoP catalyst activity for syngas conversion with time-on-stream at H_2:CO = 1 and 8.27 MPa.

the reduction reaction is somewhat uncertain because of the possible presence of polyphosphate chains [37,38] and species such as $H_xPO_4^{(x-3)}$ and P^{3+} in the calcined precursors. In addition, during calcination and reduction, some loss of P may occur through volatile phosphorous species that leave the catalyst surface during the reduction or calcination process, all of which may contribute to a higher actual degree of reduction than that calculated from the data of Fig. 1 [39].

Table 2 reports the catalyst BET surface areas as well as the catalyst surface composition as determined by XPS analysis of the reduced, passivated catalysts. The BET areas of the catalysts after reaction are also reported in Table 2. The Rh–K–MoP/SiO_2 catalyst BET area (56 m^2/g) and the K–MoP/SiO_2 catalyst (64 m^2/g) were significantly lower than that of the SiO_2 (330 m^2/g) and the 5 wt%K/SiO_2 (264 m^2/g) supports. The most significant decrease in area occurred with the addition of MoP to the K/SiO_2 support. The used catalysts all showed a decrease in surface area after reaction, mainly due to carbon deposition [31].

Previous work on K–MoP/SiO_2 catalysts has shown that the Mo:Si ratio, as determined by XPS, is a measure of the Mo dispersion [31], and this is not affected significantly by the addition of the K to the SiO_2 prior to the loading of MoP onto the support. The surface composition data of Table 2 show, however, that with the addition of Rh, there appears to be a loss in MoP dispersion. For the K–MoP/SiO_2 catalyst, the MoP dispersion was 2.8% (i.e. the Mo/Si atom ratio expressed as a percentage) whereas for the Rh–K–MoP/SiO_2 catalyst it was 1.9%. The surface of the catalysts was also enriched in Mo (Mo:P > 1, Table 2), consistent with the bulk chemical analysis, and the Mo enrichment is ascribed to the loss of surface P during thermal treatment of the catalysts.

XPS narrow scan analysis of the reduced and passivated Rh–K–MoP/SiO_2 catalyst is shown in Fig. 2. The Mo3d spectrum of Fig. 2 was de-convoluted using spin orbit splitting of 3.2 eV and three distinct $Mo3d_{5/2}$ binding energies (BEs). The low BE peak (228 eV) was assigned to MoP [39,41] whereas the higher BEs correspond to Mo^{5+} and Mo^{6+} species that result from the passivation of the catalyst [41]. The P2p spectra of Fig. 2 was de-convoluted into two peaks with BE 133 eV assigned to phosphate species and BE 126.6 eV assigned to phosphide species [41]. Although the Rh narrow scan XPS profile had a relatively high signal-to-noise ratio, a Rh $3d_{5/2}$ peak at 307.2 eV, corresponding to Rh^0 species, and a peak at 309.2 eV, corresponding to Rh^{3+}, were identified [42,43].

3.2. Comparison of catalysts

Fig. 3 compares the CO conversion measured at 548 K, 8.3 MPa and a H_2:CO ratio of 1 over the 5 wt% K–10 wt% MoP/SiO_2 and the 1 wt% Rh–5 wt% K–10 wt% MoP/SiO_2 catalyst. A sharp decrease in activity was observed for the K–MoP/SiO_2 catalyst at the beginning of the experiment, and similar behaviour was reported previously for a series of catalysts with a range of MoP and K loadings on SiO_2 [31]. However, with the addition of Rh, the activity of the catalysts stabilized, and the same catalyst stability was observed at 573 K and a correspondingly higher CO conversion.

Activity and selectivity data were averaged over the 20–60 h run time period following the initial 20 h stabilization period for the catalysts and these results are summarized in Table 3, comparing the MoP/SiO_2 catalyst product distribution obtained from synthesis gas reacted at 548 K and 8.27 MPa to that from the 5 wt% K–10 wt% MoP/SiO_2 and the 1 wt% Rh–5 wt% K–10 wt% MoP/SiO_2 catalyst. Although there was a significant increase in CO_2 selectivity with K addition to the MoP/SiO_2 catalyst, a smaller increase occurred with addition of Rh to the K–MoP/SiO_2. The addition of K to the MoP/SiO_2 catalyst suppressed the selectivity to CH_4 and increased selectivity to C_{2+} oxygenates. The 5 wt% K–10 wt% MoP/SiO_2 catalyst, operated at 548 K and 8.27 MPa, had a CH_4 selectivity of only 9.7 C atom% and a C_{2+} oxygenate selectivity of 72.6 C atom%. In previous work, the 5 wt% K–10 wt% MoP/SiO_2 catalyst was shown to give the lowest CH_4 and highest C_2 oxygenate selectivity among a series of K–MoP/SiO_2 catalysts [31]. At the same operating conditions, the present work shows that addition of 1 wt% Rh to the K–MoP/SiO_2 catalyst increased the CO conversion from 8.4 to 9.7%. The selectivity to the undesired products, CH_4 and other hydrocarbons, also increased (Table 3). A small decrease in the C_{2+} oxygenate selectivity, increase in ethanol selectivity and a decrease in acetaldehyde selectivity were also observed. The space–time yield (STY) of the C_{2+} oxygenates also decreased marginally. With the Rh–K–MoP/SiO_2 catalyst, the STY for C_{2+} oxygenate was 54.9 g kg cat.$^{-1}$ h^{-1} compared to 59.3 g kg cat.$^{-1}$ h^{-1} for the 5 wt% K–10 wt% MoP/SiO_2 catalyst [30].

Overall, the present data show that addition of Rh to the K–MoP/SiO_2 catalyst improved the stability of the catalyst compared to the K–MoP/SiO_2 catalyst. The Rh increased the selectivity to hydrocarbon products, especially CH_4, while increasing the selectivity to ethanol marginally. The addition of Rh did not appear to significantly increase the hydrogenation of acetaldehyde to ethanol.

Table 2
BET area and surface composition of catalysts as determined by XPS.

Catalyst	MoP/SiO_2	$K\text{-}MoP/SiO_2$	$Rh\text{–}K\text{–}MoP/SiO_2$
BET area, m^2/g	263	64	56
BET area after reaction, m^2/g	181	6	24
Surface composition, mole ratio			
Rh:Si	–	–	0.0026
K:Si	–	0.099	0.084
Mo:Si	0.027	0.028	0.019
P:Si	0.024	0.022	0.016
Mo:P	1.10	1.28	1.20

3.3. Activity and selectivity of the Rh–K–MoP/SiO_2 catalyst

The Rh–K–MoP/SiO_2 catalyst was evaluated at different reaction temperatures, in the range of 548–613 K, with H_2:CO feed gas ratios of 1, 1.5 and 2. At each set of operating conditions, the catalyst weight in the reactor was adjusted so as to maintain the CO conversion at approximately the same level and below 25% at each set of conditions. This experimental procedure was followed so that the micro-reactor was operated isothermally and to ensure that the observed kinetics were free of mass and heat transfer resistances. Furthermore, selectivity data reported at a fixed CO conversion are required for proper interpretation. By changing the catalyst weight at each temperature, the average CO conversion was maintained at $17.4 \pm 4.3\%$ for all the data reported herein.

The effect of temperature and H_2:CO ratio on the product selectivity obtained over the Rh–K–MoP/SiO_2 catalyst is presented in Table 4. With increased temperature and fixed H_2/CO ratio, the methane and total hydrocarbon selectivity increased, whereas the C_{3+} oxygenate selectivity decreased. The variation in ethanol and acetaldehyde selectivity was small because the data were collected over a narrow range of CO conversions. The acetaldehyde selectivity was in the range of 18.6–23.3 C atom% and the ethanol selectivity was in the range of 16.0–20.0 C atom%. Methanol selectivity increased with increase in temperature although in all cases the methanol selectivity was below 2 C atom%. Low methanol selectivity is a unique characteristic of the MoP-based catalysts, as reported previously [31]. The CO_2 selectivity showed a decreasing trend with increased temperature and increased H_2/CO ratio. The trend was most pronounced at 598 K. The water-gas-shift (WGS) reaction [$CO + H_2O \leftrightarrow CO_2 + H_2$, $\Delta H_r = -41.1$ kJ/mol] shifted to the left as H_2 partial pressure and/or temperature increased, leading to a decrease in CO_2 selectivity.

The effect of temperature and H_2:CO ratio on the STY of the individual product components is reported in Table 5. In all cases, the C_{2+} oxygenate STY increased with an increase in temperature. The effect of the H_2/CO ratio was dependent upon the reaction temperature. At 548 K there was a small increase in the C_{2+} oxygenate STY with increased H_2:CO ratio whereas at 613 K, the reverse trend was observed (the C_{2+} oxygenate STY decreased with increased H_2:CO ratio).

3.4. Reaction kinetics

The space–time yield data of the various products generated in the present study, represent the average rate of formation of each component in the reactor. Since the CO conversion levels were kept low as the temperature and H_2:CO ratio varied, the change in H_2 and CO partial pressures through the reactor bed was low (the maximum variation was $\pm 5\%$) for all the data of Table 5. Hence the space–time–yield data can be taken as an estimate of the rate of formation of each of the compounds at the average H_2 and CO partial pressures in the reactor, as reported in Table 5. These data have been used to estimate kinetic parameters for each component using simple empirical power law kinetics of the form $r = ke^{-E/RT}P_{H_2}^m P_{CO}^n$ where k is the reaction rate constant, E is the apparent activation energy and P_{H_2} and P_{CO} are the partial pressure of H_2 and CO raised to a power m and n, respectively. The power law equation was applied to each of the major components as well as the rate of CO consumption (on a CO_2 free basis) and in order to improve the confidence limit on each of the estimated parameters, the hydrogen exponent (m) was assumed to be equal to one. Previous studies that have reported empirical power law kinetics for alcohol synthesis from syngas, report H_2 exponents in the range 0.7–1.3 for methanol, ethanol and propanol [44]. For the range of conditions used in the present study, wherein the H_2 partial pres-

Table 3
Effect of promoters on synthesis gas conversion over MoP/SiO_2 catalysts.

Catalyst	MoP/SiO_2	$K\text{–}MoP/SiO_2$	$Rh\text{–}K\text{–}MoP/SiO_2$
MoP, wt%	10	10	10
K, wt%	0	5	5
Rh, wt%	0	0	1
Temperature, K	548	548	548
GHSV, h^{-1}	3960	3960	3960
H_2:CO	1.0	1.0	1.0
CO conversion, %	2.8	8.4	9.7
STY C_{2+} oxygenates, g/(kg cat h)	15.1	59.2	54.9
CO_2 selectivity, C atom%	24.8	44.9	51.4
Selectivity, C atom% excl. CO_2			
Hydrocarbons	57.3	23.4	34.9
CH_4	32.5	9.7	11.7
Methanol	0.5	4.0	0.7
Acetaldehyde	19.1	20.5	18.6
Ethanol	4.4	15.3	16.0
Propanol	2.2	7.4	6.2
Acetone	13.8	14.1	5.3
Total C_2 + oxygenate	42.6	72.6	64.4

S_{CO_2} = carbon atom% selectivity to carbon dioxide.

Table 4
Averaged product selectivities from syngas conversion over the 1%Rh–5%K–10%MoP/SiO_2 catalyst.

Temp, K GHSV, h^{-1}	H_2:CO	% CO conv.	S_{CO_2}	Selectivity (CO_2 free, C atom%)							
				HC	CH_4	MeOH	AcH	EtOH	Acetone	C_{2Oxy}	C_{3+Oxy}
548	1.0	9.7	51.4	34.9	11.6	0.7	18.6	16.0	5.3	37.1	27.3
3960	2.0	18.0	44.4	31.8	14.0	0.8	20.5	18.9	9.6	40.9	26.4
573	1.0	13.6	45.6	32.6	13.0	1.2	19.8	19.2	9.0	40.7	25.7
7920	1.5	15.6	44.9	35.4	14.9	1.2	20.8	18.3	10.1	40.7	22.6
	2.0	20.7	43.3	35.8	15.8	1.2	19.6	18.0	9.8	39.2	23.9
598	1.0	13.9	45.0	38.6	16.8	1.5	23.1	20.0	4.5	44.0	16.0
15,840	1.5	17.0	44.5	38.6	17.8	1.3	19.9	18.2	8.6	39.2	20.9
	2.0	21.3	42.7	38.3	18.9	1.2	20.9	18.3	7.6	40.5	20.0
613	1.0	19.7	43.9	40.3	18.2	1.8	21.6	19.5	5.0	41.9	16.0
15,840	2.0	24.4	42.2	42.7	21.1	1.9	23.3	18.8	3.2	42.8	12.7

S_{CO_2} = carbon atom% selectivity to carbon dioxide. HC, total hydrocarbons; AcH, acetaldehyde; ΣC_{2oxy}, sum of acetaldehyde, ethanol and acetic acid; C_{3+oxy}, acetone, propanol, butanol, propionic acid, methyl acetate, ethyl acetate; NA, data not available.

Table 5
Averaged space–time–yields of major products from syngas conversion over the 1%Rh–5%K–10%MoP/SiO_2 catalyst.

Temperature	Feed H_2/CO	Average partial pressure[a]		CO consumption, CO_2 free	Component STY					C_{2+} STY
		H_2	CO		CH_4	CH_3CHO	Methanol	Ethanol	Propanol	
K	ratio	MPa	MPa	μmol g cat^{-1} s^{-1}	μmol g cat^{-1} s^{-1}					g kg cat^{-1} h^{-1}
548	1.0	4.20	4.09	1.048	0.122	0.097	0.008	0.084	0.022	55
	2.0	5.58	2.64	1.463	0.205	0.150	0.012	0.138	0.025	79
573	1.0	4.22	4.00	3.280	0.426	0.325	0.039	0.315	0.055	174
	1.5	5.04	3.23	3.348	0.499	0.348	0.041	0.306	0.053	169
	2.0	5.58	2.55	3.426	0.541	0.336	0.041	0.308	0.053	174
598	1.0	4.22	3.99	6.777	1.130	0.783	0.100	0.678	0.093	327
	1.5	4.99	3.30	7.363	1.311	0.731	0.093	0.671	0.107	352
	2.0	5.58	2.65	7.144	1.347	0.745	0.083	0.651	0.099	345
613	1.0	4.19	3.92	9.798	1.783	1.058	0.175	0.955	0.143	454
	2.0	5.58	2.64	8.247	1.740	0.961	0.157	0.755	0.109	368

[a] Average of inlet and outlet H_2 and CO partial pressures.

sure varies over a relatively narrow range (from 4.2 to 5.6 MPa, Table 5) and for which the H_2 and CO partial pressures were highly correlated, an assumed exponent of $m = 1.0$ suffices. The unknown parameters k, E and n were evaluated by fitting the power law equation to the experimental STY data. The Marquardt–Levenberg optimization procedure was used to evaluate the parameters by minimizing the objective function $S = \sum_{i=1}^{N}(r - r_{\mathrm{mod}})^2$ where r_{exp} is the measured STY of the components of interest and r_{mod} is the STY calculated from the power law model. The kinetic parameters for the four major components are reported in Table 6 and the parity plot, shown in Fig. 4, confirmed the goodness-of-fit between the experimental observations and the model calculations. The data of Table 6 show that the apparent activation energy of the alcohols decreased as the alcohol carbon number increased. Furthermore, the activation barriers associated with the formation of acetaldehyde and ethanol were approximately equal (within the standard deviation associated with the parameter estimates), and these were both significantly lower than the apparent activation energy for methanol.

4. Discussion

The catalyst characterization data show that addition of Rh to the K–MoP/SiO_2 catalyst decreased the catalyst BET surface area

Table 6
Power law rate parameters for major products over the 1%Rh–5%K–10%MoP/SiO_2 catalyst.

Component	Power law rate expression, $r = A\exp\left(-\frac{E}{RT}\right)P_{H_2}P_{CO}^{m}$, μmol $gcat^{-1}$ s^{-1}			
	Activation energy, E kJ/mol	Power law exponent, m –	Pre-exponential factor, A (μmol) $(MPa)^{-(m+1)}$.$(s)^{-1}$	R^2 %
CO consumption[a]	75.0 ± 5.9[b]	0.74 ± 0.14	0.3898	96.1
Methane	91.3 ± 6.7	0.48 ± 0.15	0.0871	96.8
Acetaldehyde	81.9 ± 5.1	0.77 ± 0.12	0.0388	97.5
Methanol	114.5 ± 10.9	1.00 ± 0.21	0.0033	94.2
Ethanol	77.7 ± 5.1	0.93 ± 0.12	0.0288	97.1
Propanol	66.9 ± 9.9	0.79 ± 0.25	0.0055	86.3

[a] CO_2 free basis.
[b] Std. deviation of parameter estimate.

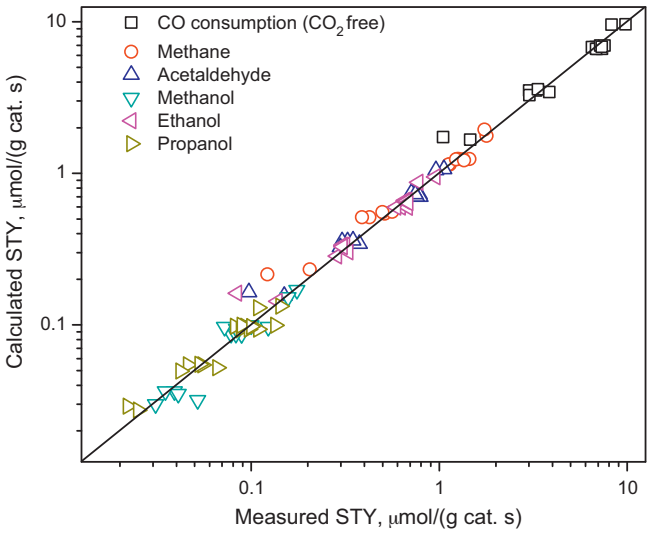

Fig. 4. Parity plot for power law kinetic models shown in Table 6.

and the MoP dispersion. This suggests that the Rh was dispersed over the support as well as the MoP, although the MoP surface concentration on the support was about 10×'s greater than that of Rh. The TPR profile of the MoP precursors was not affected by the addition of Rh and the TPR data showed that 100% of the Rh precursor was reduced to Rh metal. In addition, the BEs of the Mo and P species on the passivated Rh–K–MoP/SiO_2 catalyst were similar (within the BE resolution capability of the instrument) to those reported previously for K–MoP/SiO_2 catalysts [31]. Hence, the catalyst characterization data suggest that the Rh was dispersed over the catalyst as Rh^0 and that the presence of Rh did not influence the properties of the MoP.

In previous work, it was shown that on K–MoP/SiO_2 catalysts, both acetaldehyde and ethanol were the major C_2 oxygenated products of syngas conversion [31]. The addition of Rh to the K–MoP/SiO_2 catalyst was expected to enhance ethanol selectivity by hydrogenating the acetaldehyde to ethanol [45]. However, the data of Table 3 showed that this did not occur to any great extent. Addition of Rh increased the selectivity to CH_4 and other hydrocarbons and, to a much lesser extent, increased the selectivity to ethanol, although a small decrease in the total C_{2+} oxygenate selectivity was observed.

Several Mo-based catalysts have been investigated for CO hydrogenation to alcohols and hydrocarbons, and Table 7 summarizes some recently reported results. Table 7 shows that in the absence of alkali metal oxides, Mo, Mo_2C and MoS_2 yield mostly methane and other hydrocarbons, similar to that obtained on the MoP/SiO_2 catalyst of the present study (Table 3). Although addition of K to Mo_2C and MoS_2 catalysts decreased CO conversion, the selectivity to alcohols and other oxygenates increased while hydrocarbon selectivity was suppressed [46,47]. The data of Table 3 show similar effects with K addition to the MoP/SiO_2 catalyst, as reported previously [31].

The effect of addition of Group VIII metal promoters to the Mo-based catalysts is somewhat more complicated. Table 7 shows that the addition of Co to a K–MoS_2 catalyst decreased hydrocarbon selectivity while increasing CO conversion, C_{2+} oxygenate selectivity and alcohol STY, and similar data have been reported by others [20–22]. An increased alcohol selectivity and alcohol STY was also observed with Rh addition to a K–Mo_2S catalyst [23]. However, addition of Co to the K–Mo_2C catalyst increased CO conversion and alcohol STY but, significantly, the hydrocarbon selectivity also increased. The K–Co–Mo catalyst [49] also had high selectivity to hydrocarbons. In the present work, increased hydrocarbon selectivity was also observed with Rh addition to the K–MoP/SiO_2 catalyst. Together, these results show that the Group VIII metal added to Mo, Mo_2C and MoP catalysts behave differently compared to when they are added to the MoS_2 catalysts. In the latter case, especially when the catalysts are pre-treated in H_2S, the Group VIII metals are readily sulphided [47], whereas in the case of Mo, Mo_2C and MoP, there is no exposure to S. In the case of Rh, Koizumi et al. [47] has shown that sulphided Rh species ($Rh_{17}S_{15}$) have high methanol selectivity and overall alcohol selectivity significantly greater than the hydrocarbon selectivity. Similarly, when MoS_2 is promoted with Co, the surface species include a Co_8S_9 species [54] and the K–Co–MoS_2 catalyst also has increased yield of alcohols compared to K–MoS_2 catalysts. Hence we conclude that the effect of Group VIII metal promotion of MoS_2 catalysts results in at least partially sulphided species whereas in the case of Mo, Mo_2C and the MoP of the present work, the Co and Rh remain in a metallic state, and for this reason the hydrocarbon selectivity increases on these catalysts.

The hydrogenation capabilities of the Rh present in the Rh–K–MoP/SiO_2 catalyst is also likely responsible for the improved stability of the catalyst compared to the K–MoP/SiO_2 catalyst. As noted previously [31], the deactivation of these catalysts is linked to carbon deposition from heavy products or carbon generated by the Boudouard reaction. In either case, improved hydrogenation of the catalyst would be expected to reduce the carbon deposition by hydrogenation to methane or other light hydrocarbons, and thereby improve catalyst stability.

The MoP catalysts of the present study show promise for several reasons. Firstly, MoP has higher selectivity to ethanol compared to Mo_2C, MoP has higher C_{2+} oxygenate selectivity than other Mo-based catalysts (Tables 3 and 7) and the products are not contaminated with S as in the case of MoS_2 [44]. The MoP catalysts also have relatively low hydrocarbon selectivity. In addition, in most other alcohol synthesis catalysts, (MoS_2, Mo_2C, Cs–Cu–ZnO, modified FT catalysts) methanol is the major or second major liquid

Table 7
Effect of promoters on Mo-based catalysts for synthesis gas conversion.

Catalyst	MoS_2				Mo_2C			Mo	
Promoters	–	K	K–Co	K–Rh	–	K	K–Co	–	K–Co
Reference	[55]	[48]	[48]	[23]	[47]	[47]	[56]	[49]	[49]
Temperature, K	613	583	583	600	573	573	573	503	503
GHSV, h^{-1}	6000	4800	4800	4800	2000	2000	2000	4800	4800
H_2:CO	2.0	2.0	2.0	2.0	1.0	1.0	1	2.0	2.0
Pressure, MPa	4.1	5.0	5.0	10.0	8.0	8.0	8	5.0	5.0
CO conversion,%	50	5	15	11	59	23	51	0.3	12
CO_2 selectivity, C atom%	42	20	26	–	52	50	–	–	–
Selectivity, C atom% excl. CO_2									
Hydrocarbons	100	57	16	41	96	47	60	100	51
Methanol	0	24	26	11	3	19	11	0	6
Total C_{2+} oxygenate	0	20	58	48	1	34	29	0	43
Alcohol STY, g/(kg cat h)	0	31	189	174	16	122	161	0	185

product [1,2], whereas for the MoP catalyst, methanol selectivity was the lowest among the C_1–C_3 oxygenated products. A low selectivity to methanol also occurs on Rh-based catalysts [12,14,15,45].

On MoP and MoS_2 catalysts, CO is adsorbed non-dissociatively [29]. DFT studies of an Mo_6P_3 cluster model of MoP [50] identified the reaction mechanism for synthesis gas conversion to methane as:

$$CO_{ad} \xrightarrow{H} CHO_{ad} \xrightarrow{H} CH_2O_{ad} \xrightarrow{H} CH_2OH_{ad} \xrightarrow{H} CH_{2.ad} + H_2O \xrightarrow{H} CH_{3.ad} + H_2O \xrightarrow{H} CH_4 + H_2O$$

and for methanol synthesis as:

$$CO_{ad} \xrightarrow{H} CHO_{ad} \xrightarrow{H} CH_2O_{ad} \xrightarrow{H} CH_2OH_{ad} \xrightarrow{H} CH_3OH$$

Similar mechanisms involving the same surface intermediates have also been reported for MoS_2 catalysts [51]. On MoP the C–O bond breaks upon H_{ad} addition to the O of the hydroxymethylene (CH_2OH_{ad}) species, forming $CH_{2.ad}$ and H_2O_{ad}. The CH_2 species participate in CO insertion reactions or other C–C bond forming reactions with other surface species to yield higher oxygenates [45]. DFT studies on the Mo_6P_3 cluster model of MoP identified the formation of methanol from hydroxymethylene (CH_2OH) or methoxy (CH_3O) adsorbed species as having a much higher activation barrier than C–O bond breakage of hydroxymethylene to produce the CH_2 species. Accordingly, the activation barrier for C_{2+} oxygenated products would be expected to be less than that for methanol formation. The apparent activation energies reported in Table 6 support these modeling results in that they show a higher apparent activation energy for methanol formation than for either ethanol, acetaldehyde or propanol formation.

The apparent activation energies estimated for ethanol and acetaldehyde formation on the Rh–K–MoP/SiO_2 catalyst were very similar (Table 6), suggesting that a common intermediate is involved in the kinetic steps leading to these products. Most kinetic models of ethanol synthesis on Rh favour a mechanism in which ethanol is produced by the secondary hydrogenation of acetaldehyde, and assume that ethanol and acetaldehyde are formed through a common pathway [1,45]. For the present catalyst, however, acetaldehyde was not hydrogenated to ethanol as the H_2:CO ratio increased and both acetaldehyde and ethanol were significant products over the K–MoP/SiO_2 and the Rh–K–MoP/SiO_2 catalysts. The MoP does not show the hydrogenation ability to convert acetaldehyde to ethanol that is apparent on Rh catalysts.

On Rh-based catalysts the reaction begins with CO dissociation and hydrogenation to yield CH_x species which then undergo hydrogenation to CH_4 as well as CO insertion and hydrogenation to yield higher alcohols and hydrocarbons [45]. The increase in hydrocarbon selectivity observed upon Rh addition to the K–MoP/SiO_2 catalyst suggests that Rh hydrogenated adsorbed CH_2 species to produce methane or higher hydrocarbons and these species likely resided on the Rh, but may also have originated from the MoP. However, the relatively low selectivity to hydrocarbons obtained over the K–MoP/SiO_2 catalyst suggests that there are relatively few of these species on the MoP catalyst. On the other hand, the fact that the acetaldehyde selectivity decreased and ethanol selectivity increased only marginally with addition of Rh to the K–MoP/SiO_2 catalysts, is indicative of oxygenated surface species, mostly on the K–MoP catalyst that do not migrate to Rh, and hence do not undergo further hydrogenation.

The activation energy for methane formation on a Rh–CeO_2/SiO_2 catalyst was reported as 92.5 kJ/mol [15], for a 1%Rh/SiO_2 catalyst [14] a value of 94.6 kJ/mol has been reported and on a 1%Rh/ZrO_2 catalyst a value is 134.6 kJ/mol has been reported [52,53]. The Rh–K–MoP/SiO_2 catalyst of the present study had activation energy of 91.3 kJ/mol for methane formation. The relatively similar values of the activation energies for methane formation suggest that on the Rh–K–MoP/SiO_2 catalyst, a significant fraction of the methane formed on the Rh surface. For the same series of catalysts, the activation energy for ethanol formation was reported as 49.4 kJ/mol on Rh–CeO_2/SiO_2 and 66.5 kJ/mol on 1%Rh/ZrO_2. On the Rh–K–MoP/SiO_2 catalyst the activation energy is significantly higher at 77.7 kJ/mol, suggesting that ethanol and other oxygenates are mainly formed on the K–MoP species of this catalyst, rather than on the Rh.

5. Conclusions

The MoP catalysts showed a distinct product distribution compared to other Mo-based catalysts for syngas conversion. Low selectivity to methanol and moderate selectivity to a mixture of C_2 oxygenates (acetaldehyde, ethanol and acetic acid) was achieved on the K–MoP–SiO_2 and the Rh–K–MoP/SiO_2 catalysts. Addition of Rh to the K–MoP/SiO_2 catalyst improved the stability of the catalyst compared to the K–MoP/SiO_2 catalyst. However, the Rh increased the selectivity to hydrocarbon products, especially CH_4, while only increasing the selectivity to ethanol marginally. The results suggest that the oxygenated products were mainly produced on the K–MoP surface. The empirical power law kinetic parameters suggested a common reaction intermediate for ethanol and acetaldehyde. Hydrogenation of acetaldehyde to ethanol did not occur to any great extent, even in the presence of the Rh.

Acknowledgement

Financial support from the Natural Science and Engineering Research Council (NCERC) of Canada is gratefully acknowledged.

References

[1] V. Subramani, S.K. Gangwal, Energy Fuels 22 (2008) 814.
[2] J.J. Spivey, A. Egbebi, Chem. Soc. Rev. 36 (2007) 1514.
[3] G.D. Graves, Ind. Eng. Chem. Res. 23 (1931) 1381.
[4] P.K. Frolich, D.S. Cryder, Ind. Eng. Chem. Res. 22 (1930) 1051.
[5] W.H. Chen, H.H. Kung (Eds.), Methanol Production and Use, Marcel Dekker Inc., New York, 1994.
[6] A. Beretta, E. Tronconi, P. Forzatti, I. Pasquon, E. Micheli, L. Tagliabue, G.B. Antonelli, Ind. Eng. Chem. Res. 35 (1996) 2144.
[7] K.J. Smith, R.B. Anderson, Can. J. Chem. Eng. 61 (1983) 40.
[8] R.G. Herman, Catal. Today 55 (2000) 233.
[9] K.J. Smith, R.B. Anderson, J. Catal. 85 (1984) 428.
[10] P. Chaumette, Ph. Courty, A. Kiennemann, B. Ernst, Top. Catal. 2 (1995) 117.
[11] J. Hu, Y. Wang, C. Cao, D.C. Elliott, D.J. Stevens, J.F. White, Catal. Today 120 (2007) 90.
[12] Z. Fan, W. Chen, X. Pan, X. Bao, Catal. Today 147 (2009) 86.
[13] A. Egbebi, J.J. Spivey, Catal. Commun. 9 (2008) 2308.
[14] C. Mazzocchia, P. Gronchi, A. Kaddouri, E. Tempesti, L. Zanderighi, A. Kiennemann, J. Mol. Catal. A: Chem. 165 (2001) 219.
[15] H. Trevino, T. Hyeon, W.M.H. Sachtler, J. Catal. 170 (1997) 236.
[16] M. Ichikawa, T. Fukushima, J. Chem. Soc. Chem. Commun. (1985) 321.
[17] S.T. Oyama, J. Catal. 216 (2003) 343.
[18] Q.J. Quarderer, G.A. Cochram, US Patent WO84/03696, 1984.
[19] R.R. Stevens, US Patent 4882360, 1989.
[20] J. Iranmahboob, D.O. Hill, T. Hossein, Appl. Catal. A: Gen. 231 (2002) 99.
[21] H. Qi, D. Li, C. Yang, Y. Ma, W. Li, Y. Sun, B. Zhong, Catal. Commun. 4 (2003) 339.
[22] D. Li, C. Yang, H. Qi, H. Zhang, W. Li, Y. Sun, B. Zhong, Catal. Commun. 5 (2004) 605.
[23] Z. Li, Y. Fu, M. Jiang, Appl. Catal. A: Gen. 187 (1999) 187.
[24] M. Xiang, D. Li, W. Li, B. Zhong, Y. Sun, Fuel 85 (2006) 2662.
[25] M. Xiang, D. Li, H. Xiao, J. Zhang, H. Qi, W. Li, Y. Sun, Fuel 87 (2008) 599.
[26] K.J. Smith, R.G. Herman, K. Klier, Chem. Eng. Sci. 45 (1990) 2639.
[27] A.K. Gunturu, L.E. Kugler, J.B. Cropley, B.D. Dadyburjor, Ind. Eng. Chem. Res. 37 (1998) 2107.
[28] T.Y. Park, I.S. Nam, Y.G. Kim, Ind. Eng. Chem. Res. 36 (1997) 5246.
[29] M. Huang, K. Cho, J. Phys. Chem. C 113 (2009) 5238.
[30] S.F. Zaman, K.J. Smith, Catal. Comm. 10 (2009) 468.
[31] S.F. Zaman, K.J. Smith, Appl. Catal. A: Gen. 378 (2010) 59.
[32] P.A. Clark, S.T. Oyama, J. Catal. 218 (2003) 78.
[33] V. Zuzaniuk, R. Prins, J. Catal. 219 (2003) 85.
[34] R. Thomas, J.A. Moulijn, V.H.J. De Beer, J. Medema, J. Mol. Catal. 8 (1980) 161.
[35] H. Trevino, G.-D. Lei, W.M.H. Sachtler, J. Catal. 154 (1995) 245.
[36] L. Huang, W. Chu, J. Hong, S. Luo, Chin. J. Catal. 27 (2006) 596.
[37] C. Stinner, R. Prins, T. Weber, J. Catal. 191 (2000) 438.

[38] C. Stinner, R. Prins, T. Weber, J. Catal. 202 (2001) 187.
[39] I.I. Abu, K.J. Smith, J. Catal. 241 (2006) 356.
[40] I.I. Abu, K.J. Smith, Appl. Catal. A: Gen. 328 (2007) 58.
[41] D.C. Phillips, S.J. Sawhill, R. Self, M.E. Bussell, J. Catal. 207 (2002) 266.
[42] D.K. Ghori, R.M. Sanyal, B. Sen, S.K. Ghosh, K.C. Banerji, E.S. Shpiro, K.M. Minachev, React. Kinet. Catal. Lett. 40 (1989) 259.
[43] C. Force, E. Roman, J.M. Guil, J. Sanz, Langmuir 23 (2007) 4569.
[44] J.M. Christensen, P.M. Mortensen, R. Trane, P.A. Jensen, A.D. Jensen, Appl. Catal. A: Gen. 366 (2009) 29.
[45] S.C.C. Chuang, R.W. Stevens, R. Khatri, Top. Catal. 32 (2005) 225.
[46] M. Xiang, D. Li, W. Li, B. Zhong, Y. Sun, Catal. Commun. 8 (2007) 503.
[47] N. Koizumi, K. Murai, T. Ozaki, M. Yamada, Catal. Today 89 (2004) 465.
[48] J. Bao, Y. Fu, G. Bian, Catal. Lett. 121 (2008) 151.
[49] J. Bao, Z.-H. Sun, Y.-L. Fur, G.Z. Bian, Y. Zhang, N. Tsubaki, Top. Catal. 52 (2009) 789.
[50] S.F. Zaman, K.J. Smith, Mol. Simul. 34 (2008) 1073.
[51] X. Shi, H. Jiao, K. Hermann, J. Wang, J. Mol. Catal. A: Chem. 312 (2009) 7.
[52] F. Solymosi, M. Pasztor, J. Phys. Chem. 90 (1986) 5312.
[53] F. Solymosi, M. Pasztor, J. Phys. Chem. 89 (1985) 4789.
[54] Z. Li, Y. Fu, M. Jiang, Appl. Catal. A: Gen. 220 (2001) 21.
[55] N. Koizumia, G. Bian, K. Muraia, T. Ozakia, M. Yamada, J. Mol. Catal. A: Chem. 207 (2004) 173.
[56] M. Xiang, D. Li, W. Li, B. Zhong, Y. Sun, Catal. Commun. 8 (2007) 513.